A Study of Geostrophy in Tropical Pacific Ocean Currents during the NORPAX Tahiti Shuttle using a Shipboard Doppler Acoustic Current Profiler

ERIC S. JOHNSON, LLOYD A. REGIER AND ROBERT A. KNOX

Scripps Institution of Oceanography, University of California, San Diego, La Jolla, California

ABSTRACT

Continuous velocity measurements from a shipboard Doppler acoustic log on the NORPAX shuttle experiment in the central equatorial Pacific are presented. The time mean of these velocities shows the classical zonal equatorial currents as well as their meridional circulation. The velocities are used with concurrent CTD data to examine the geostrophic balance of zonal currents in the upper 117 m. Estimates of the errors of the acoustic data are produced from a comparison between that data and concurrent profiling current-meter data, and are used to establish the reliability of the balances observed. Both the time mean and the time varying balances are investigated, as well as the departures from geostrophic balance. The mean zonal velocities between 4°S and 10°N are found to be in approximate geostrophic balance. Departures from geostrophy in the mean are observed near the surface at the equator. The meridional advection of meridional momentum appears to be only partly responsible for this departure. The time varying flow was partly geostrophic poleward of 1°, but not so equatorward. A large excess of geostrophic velocity variance (relative to observed velocity variance) exists near the equator, probably due to high frequency internal wave signals in the density data. North of 4°N an excess of observed velocity variance was found, due probably to near-inertial waves. In both latitude bands the fluctuating departures from geostrophy are probably balanced by meridional acceleration. More than sufficient acceleration exists near the equator to account for the observed imbalance, while in the North Equatorial Countercurrent the acceleration is barely sufficient, implying a close balance between acceleration and nongeostrophic pressure gradients.

1. Introduction

The degree of meridional geostrophic balance prevailing near the equator has been a matter of interest for some time, both as a factor in models of tropical ocean circulation and as a possible aid in monitoring the predominantly zonal currents in that area of the ocean. Previous investigations involving only a few sections across the equator have found the Equatorial Undercurrent (EUC) to be variously in (Knauss 1960; Hisard et al. 1970) or out (Knauss 1966) of geostrophic balance. Lukas and Firing (1984) have shown with profiling current meter (PCM) data from the NORPAX experiment that the zonal flow within 4° latitude of the equator is roughly geostrophic in the mean of 42 sections scattered over a year and a half of time. Here data from a Doppler acoustic log (DAL) during the same experiment are presented. It consists of profiles of water velocity as a function of depth taken at 2 km intervals while the ship was underway. The DAL data, combined with the CTD profiles, are used to show that there is a rough mean geostrophic balance from 4°S to 10°N, and the departures from geostrophy are compared to other momentum terms. A comparison between the DAL and the PCM data resulting in error estimates for each is given in an appendix.

The NORPAX Hawaii to Tahiti Shuttle Experiment (Wyrtki et al. 1981) purposed in part to test our ability

to estimate currents near the equator using geostrophic calculations and to compare other schemes of measuring the currents directly. The experiment consisted of fifteen approximately monthly legs by various ships, generally on the cruise track shown in Fig. 1; the DAL was operated on the final ten legs. CTD stations were occupied every 1° of latitude along the track; PCM measurements were taken on station every 1° of latitude between 6°S and 10°N, with the sampling density increased to every 0.5° from 3°S to 3°N (Firing et al. 1981). The DAL ran continuously, providing a dense sampling of velocities along the ship's track. The ship's track was traversed in alternate directions, so the above data are unevenly sampled in time. In addition to the shipboard data collection efforts, a set of three moorings with vector averaging current meters was maintained at 0°40'N, 153°W; 0°40'S, 153°W; and 0°, 152°W (Knox and Halpern 1982).

2. The Doppler acoustic log data (DAL)

The DAL used was developed by AMETEK/Straza; it is an improved version of the modified ship's log used by Regier (1982a). It has identical transmission characteristics, transmitting 20 ms pulses of 300 kHz sound along four narrow beams. The beams are directed forward, aft, to port, and to starboard, all angled into the water 60° from the horizontal. The acoustic energy, reflected back to the instrument from supposedly passively-drifting scatterers in each beam, shows a Doppler-shift proportional to the water velocity along the beam. The Doppler-shift of the fore and the aft

Corresponding author address: Dr. Eric S. Johnson, Scripps Institution of Oceanography, NORPAX-A030, University of California, San Diego, La Jolla, CA 92093.
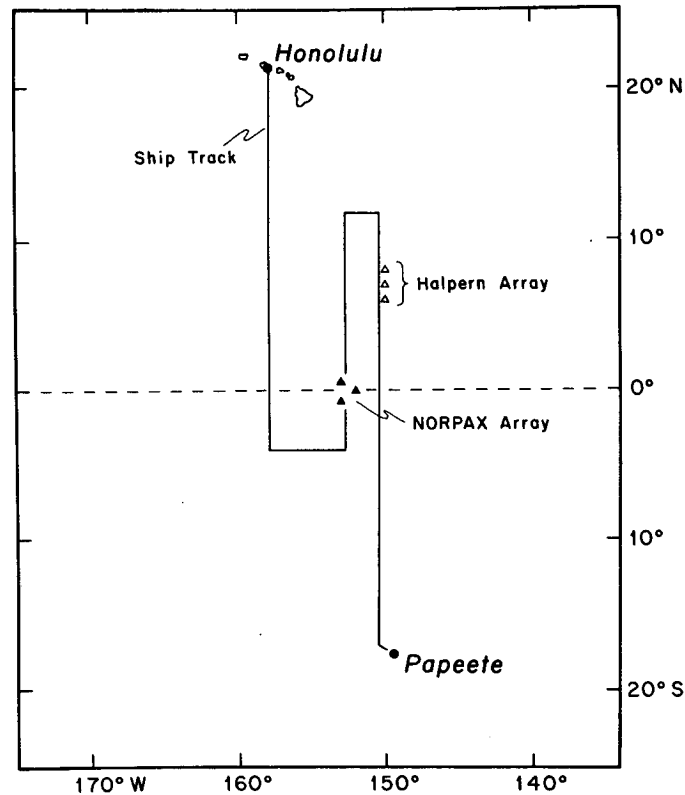
FIG. 1. The location of the NORPAX Hawaii-to-Tahiti Shuttle Experiment, showing the ship track and the location of the three NORPAX moorings, as well as those set by Halpern in the NECC.

beams are differenced to give a number proportional to the forward horizontal velocity component relative to the ship; the vertical velocity cancels in the difference. Similarly the difference of the port and starboard Doppler-shift give the starboard component of velocity. The present instrument is much improved from Regier's (1982a) instrument. In addition to improved signal processing of the acoustic returns, the instrument provides velocity estimates in up to 32 depth cells of 6.5 meters width starting at a depth of 13 m. The estimates obtained in every second cell are independent. The instrument evaluates the quality of each return echo at each depth and rejects values considered unusable. Throughout this experiment the instrument provided velocity data to a depth of 120 m. The data was recorded as block averages of 500 pings (about 5 minutes of data). This reduces both the data volume and the instrumental ping to ping noise of some 10 cm s^{-1} rms.

The data used here has been subjected to a number of cleaning processes to remove errors unique to this instrument. False returns apparently from the ship's hull biased towards zero the velocities in the upper two depth bins, preventing their use. The shallowest usable bin is at 26 m depth. In some areas, notably the North Equatorial Counter Current (NECC), low quality returns from unexpectedly shallow depths escaped the instrument quality control system and were inadvertently included in the block averages; such data was subsequently eliminated. Finally the digitally recorded data included a quantity of single bit dropouts of unknown origin which were corrected or discarded.

Unrecoverable errors exist in the data due to the wave induced motion of the ship. These are in general either small, or random and therefore mitigated by averaging. An exception is the effect of the roll and pitch of the ship displacing the acoustic beams. This reduces the measured velocity by a factor of the cosine of the roll angle, and also shifts the apparent depth of velocity features downward slightly. Averaging over several rolls smears features in the vertical in addition to shifting them downward. This effect should be of little significance during the NORPAX shuttle. Measurements taken during leg 6 indicate a rms roll angle of 3°. Typical extreme roll angles of 5°, or at most 10°, would correspond to vertical smearing over 10%–21% of the depth of the measurement. At the extreme depth range this is comparable to the 13 m averaging employed by the instrument.

The cleaned relative velocity data was rotated into geographical coordinates using the ship's heading recorded automatically every two minutes. Gaps in the

heading time series were filled from the ship's bridge log. The latter was available with much less frequency, but this lack introduced only small additional errors due to the uniformity of the ship's heading between stations. Small heading errors can alias significant amounts of the ship's forward velocity into the athwartships (zonal) component; for this reason data taken while the ship was on station or maneuvering is not used here. This also eliminates contamination by acoustic returns from instruments over the side.

The velocity sections can be checked for erroneous zonal velocities produced by a heading bias as outlined above. Since the tracks were traversed in alternate directions, the erroneous velocities can be distinguished both from the mean flow and from random ocean variability. The estimated bias is 5 cm s^{-1} (positive for a northward track) with a standard error of 1.5 cm s^{-1}. This corresponds to a heading bias of $-0.4°$, or more probably a transducer alignment offset to $+0.4°$. The 5 cm s^{-1} signal is only 4% of the observed variance.

Knowledge of the ship's velocity relative to the earth allowed the rotated DAL relative velocities to be converted to geographical or absolute velocities. Unfortunately the ship's velocity can only be determined as an average velocity (or time integrated velocity, i.e., displacement) between sequential TRANSIT satellite fixes. These occur infrequently, typically 3–4 times per degree of latitude. Therefore, accurate absolute velocities are available only for relatively long averaging periods. Regier (1982b) estimates the rms velocity error from the fixes to be 4 cm s^{-1} for a two hour (or 40 km at a ship speed of 10 knots) period. Calculation of absolute velocities is further obstructed by DAL data gaps between many pairs of fixes, usually due to a lack of heading information in the ship's log during stations. These gaps interrupt the time integration of DAL relative velocities between fixes, making the calculation of absolute velocities between that pair of fixes impossible.

The calibration of the Doppler instrument is dependent on the speed of sound in the water surrounding the transmitter/receiver. Snell's law implies that sound speed differences elsewhere in the water column do not affect the Doppler measurement. Errors due to incorrect sound speeds are incorporated into the absolute water velocity component in the direction of the ship's motion, here the meridional velocity, where they can be significant. Shears remain relatively unaffected, as the large velocity of the ship is not a factor in their calculation. The present data was corrected for the effect water temperature on sound speed, the major factor in this area. Interpolation from the two neighboring CTD stations provided estimates of temperature at the instrument depth sufficiently accurate to reduce the maximum error to less than 1 cm s^{-1}. The effect of salinity was negligible, amounting to a 0.5 cm s^{-1} error in absolute velocity for a 1‰ salinity change. Variations in sound speed will also affect the nominal depth of a
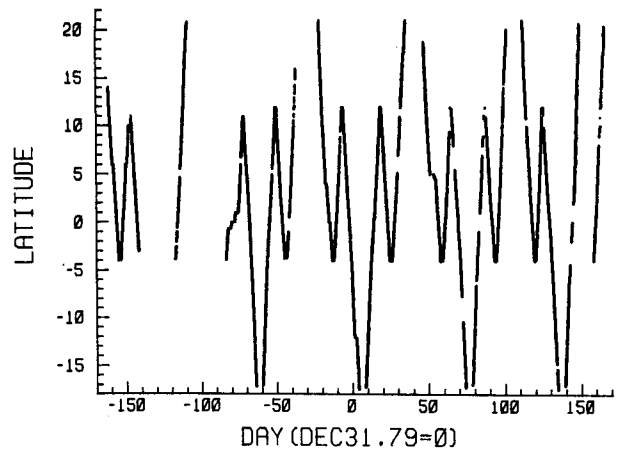

FIG. 2. The location of usable DAL data (five-minute averages) in time and latitude.

measurement, but this is neglected as a 10°C change (typical between the NECC and the equator) produces only a 2% depth error.

The DAL data is compared to the PCM and moored current meter (MCM) data in the Appendix. This comparison allows accurate error estimates to be assigned to the data. These estimates are available in Table 2 in the Appendix.

3. Results

Twenty-six meridional sections of usable DAL data were obtained between August 1979 and June 1980 (Fig. 2). These sections are distributed over the three nominal sampling longitudes of 150°, 153° and 158°W. All are grouped together and considered comparable here. No statistically significant differences can be discerned between the mean velocities at individual longitudes. Wyrtki and Kilonsky (1984) reached a similar conclusion about longitudinal gradients of temperature. Some mean differences exist, however, which are probably real: the Equatorial Undercurrent above 120 m and the South Equatorial Current (SEC) at 2°N are both 10–20 cm s^{-1} weaker at 158°W than at 153° or 150°W; the North Equatorial Countercurrent core shifts northward 1° from 158° to 150°W; the thermocline rises 10–20 m over the same interval; and the surface meridional velocity maximum at about 4°N shifts from 3°N, 158°W to 5°N, 150°W. These differences represent only small variations on the overall mean current and density fields. The variance of zonal velocity does differ significantly over longitude, increasing eastward such that the mean variance at 150°W (averaged over all depths and from 4°S to 10°N) is 1.5 times that at 158°W, with most of the increase concentrated in the region from 4°S to 4°N. An EOF analysis showed that the first three modes of variability at each longitude are spatially quite similar. Therefore, it is unlikely that different processes dom-

inate at different longitudes, and the longitudes are still considered comparable here.

The data are presented as meridional sections between 4°S and 10°N, averaged over one degree of latitude. The one degree averaging occurs between adjacent integral latitudes. This is the averaging scheme comparable with the geostrophic velocities calculated later, and results in mean velocity profiles almost indistinguishable from those produced by averaging in blocks centered on integral latitudes. About 50 five-minute average profiles are averaged into each 1° band.

The unweighted means over all longitudes and times of zonal (u) and meridional (v) velocities are presented in Fig. 3; the mean density structure obtained from CTD measurements during the same sections is shown in Fig. 4. The Equatorial Undercurrent appears roughly centered at the equator, and the North Equatorial Countercurrent has a velocity maximum at 70 m depth at 6.5°N. The mean profile of u closely resembles those of Firing et al. (1981) and Lukas and Firing (1984) over the common latitude and depth range, even
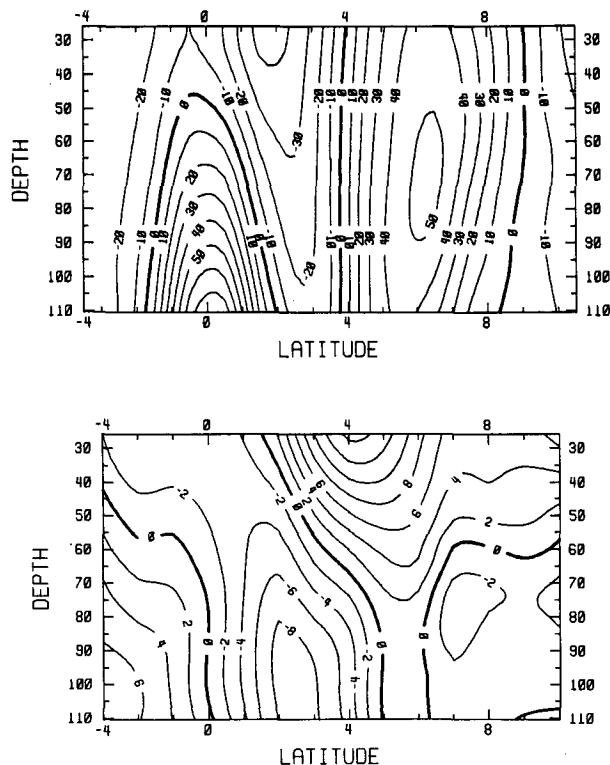

FIG. 4. The mean, as in Fig. 3, of density (σ_θ) from CTD stations at integral latitudes.

FIG. 3. The mean over all longitudes and times of DAL velocities, in cm s⁻¹. Zonal velocity (a) is positive eastwards, and meridional velocity (b) is positive northwards. Velocities separated by 1° latitude or 13 m depth are independently measured in general, although here meridional velocity has been additionally smoothed in latitude by a 2° boxcar. In this and following figures data do not extend to the surface as noted in section 2. The contouring routine contoured a smooth surface which had been fitted to the data points using cubic splines.
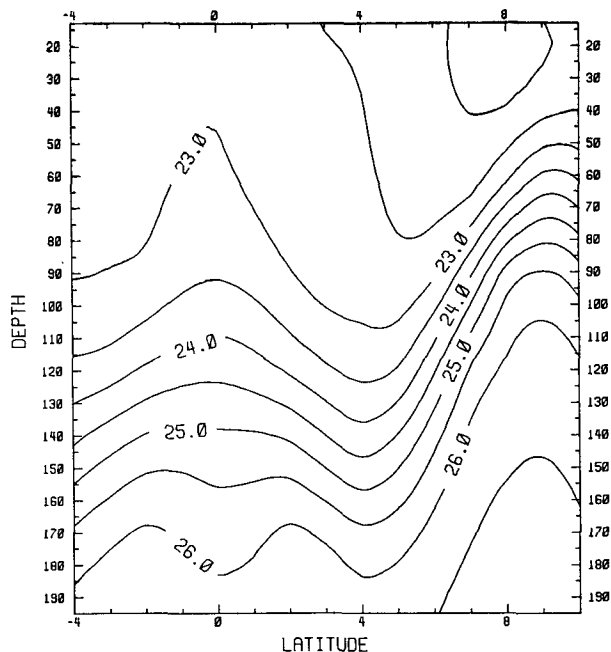
though their mean profiles include additional data from February through July, 1979. The mean profile of v closely resembles the classical equatorial circulation discussed by Wyrtki and Kilonsky (1984). There is strong convergence at and above the core of the EUC, and divergence at the surface. Note that here surface refers to the shallowest data at 26 m depth. The surface divergence appears centered at 2°–3°N. Presumably this convergence/divergence produces strong upwelling at the equator. Water from the surface divergence continues north as an Ekman drift, converging again just south of the NECC velocity maximum. This convergence forms the equatorial ridge in sea surface topography, which appears as a troughing of isopycnals around 4°–6°N in Fig. 4. Ultimately this convergence and a divergence further north (which is apparently poorly observed in Fig. 3b) produce the steeply sloped isopycnals which characterize the NECC. The region of deeper equatorward velocity extends only to 5°N, north of which v is small below 70 m. Since the convergence of the surface Ekman flow and attendant downwelling also occur north of 5°N, none of the downwelled water can recirculate back into the core of the EUC contrary to the expectations of Wyrtki and Kilonsky (1984). Nor could water masses from the north penetrate further south than about 6°N at 100 m depths. These last two conclusions must be somewhat tentative, since the standard error of the mean in Fig. 3b ranges from 4 cm s⁻¹ at 2°N to 2 cm s⁻¹ at the poleward extremes. This is enough to obscure weak southward velocity at 6°N and 100 m depth.
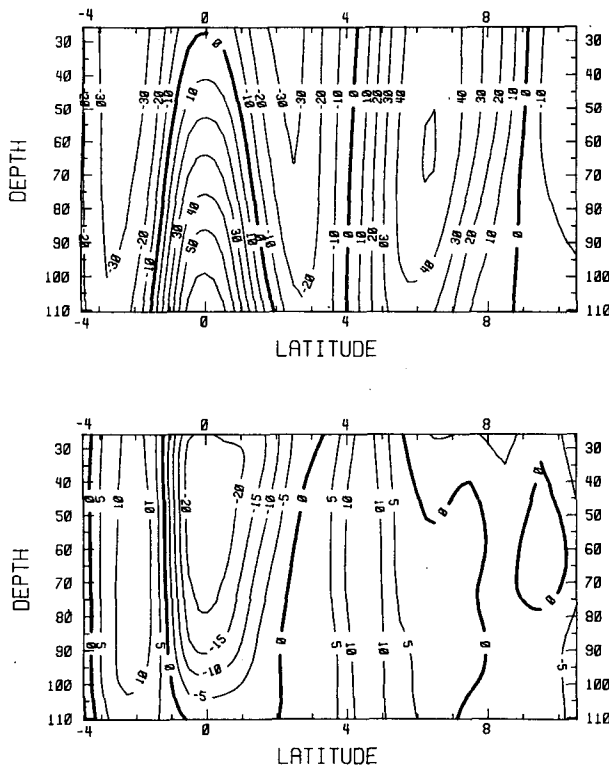
Figure 5a shows the mean zonal geostrophic velocities derived from the geostrophic relation applied between neighboring CTD stations at integral latitudes. The horizontal pressure gradient averaged from 300 to 500 m depth is assumed to be zero, as in Lukas and Firing (1984). The difference between the mean observed and geostrophic velocities, or mean ageostrophic velocity, is shown in Fig. 5b. The geostrophic and ageostrophic velocities are derived as follows. Begin with the geostrophic balance,

$$-f\Delta + fu = \frac{-1}{\rho_0} P_y,$$

where Δ is the difference between the observed zonal velocity u and the geostrophic value, and other notation is standard. To use discrete CTD stations for density (pressure) information, one must in effect integrate horizontally between stations:

$$-\int_{y_1}^{y_2} f\Delta \, dy + \int_{y_1}^{y_2} fu \, dy = \int_{y_1}^{y_2} \frac{-1}{\rho_0} P_y \, dy$$

$$= \frac{-1}{\rho_0} [P(y_2) - P(y_1)], \quad (3.1)$$

where y_1 and y_2 are the positions of two adjacent CTD

FIG. 5. The mean, as in Fig. 3, of (top) geostrophic zonal velocity relative to 300–500 m from CTD densities, and (bottom) the difference of the DAL observed (Fig. 3a) less the geostrophic velocity. Units are cm s^{-1}.

stations. As the data is recorded in time rather than space, the integrations are actually performed in time. The time averaged velocity

$$\bar{u} = \frac{1}{t_2 - t_1} \int_{t_1}^{t_2} u(t) dt,$$

can be transformed to a space average with a variable change, $y = Vt$;

$$\bar{u} = \frac{\bar{V}}{y_2 - y_1} \int_{y_1}^{y_2} \frac{1}{V} u(y) dy.$$

The space average is weighted by the inverse of the ship's velocity V, which may not be constant in time. For reasons stated in section 2, only data taken while the ship was steaming between stations are used. Hence V above is almost constant, and will cancel through the integration. Some residual effect will remain, however. The calculation of absolute water velocities (i.e., $\bar{u}$) between adjacent satellite fixes can lump water velocity measurements [i.e., $u(y)$] taken on station with those taken underway, making the station locations more heavily weighted in the integration. Similarly, absolute water velocities near the edges of a 1° averaging block may depend in part on data taken slightly outside the 1° block, depending on the location of the fixes.

As nothing more about Δ can be known than its weighted mean, take it as constant for simplicity, so that

$$\Delta = \frac{1}{\bar{f}(y_2 - y_1)} \int_{y_1}^{y_2} fu \, dy$$

$$- \frac{-1}{\rho_0 \bar{f}(y_2 - y_1)} [P(y_2) - P(y_1)] \quad (3.2)$$

where $\bar{f}$ is the average f between y_1 and y_2. The term on the right of (3.2) is the geostrophic velocity calculated from CTD data. The continuous profiling of the DAL allows the integral of fu to be calculated very accurately; each 5-minute (or 2 km at a ship speed of 10 knots) record average was multiplied by the f for the average position during that record period. This resulted in 10%–30% differences from unweighted averaging in the one-degree sections next to the equator. Of more importance, the continuous profiling eliminates the aliasing of small scale velocity features inherent in the use of only a few discrete measurements to approximate the continuous integral of u. Note also that spatial aliasing of the density (pressure) field is not a source of error in the geostrophic calculation (3.2), which depends only on the pressures at the ends of the averaging block. Δ then is an accurate measure of the actual ageostrophic velocity component.

Errors in the measurement of Δ arise both from the observations of u and from the geostrophic velocity calculation. The estimated error in the block average (i.e., integral) of u is 14 cm s^{-1} rms (see the Appendix).

Of the total, less than 3 cm s^{-1} rms is from fluctuations in ship velocity (assuming 20% fluctuations correlated over 20 km), and less than 4 cm s^{-1} rms is from satellite fixes occurring on station or beyond the averaging block. In addition there are errors due to time fluctuations of u and P during the 6 h it takes to complete a profile over 1° of latitude. The u errors are probably small. Hayes (1982) estimates that dynamic height can vary by 1.1 cm at the equator over 24 h. If one can expect 0.25 cm variations over 6 h near the equator, then resulting geostrophic velocity error is 25 cm s^{-1} rms in the 1° blocks next to the equator. Dynamic height errors due to CTD measurement uncertainties in T, S and P (0.001°C, 0.003‰, and 1 db; all assumed to be calibration errors and therefore constant with depth) amount to 0.5 cm rms, with the P errors dominating. This adds 50 cm s^{-1} to the geostrophic velocity errors next to the equator, for a total of 56 cm s^{-1}. At higher latitudes where f is larger this error will be proportionately smaller. At 2° the geostrophic error is equal to the u contribution of 14 cm s^{-1}.

The geostrophic and ageostrophic velocities derived above are further averaged between 1°S and 1°N. This is equivalent to using the equatorial geostrophic balance, and is discussed in section 5a.

Figures 3a and 5a show that the mean zonal velocity is in approximate geostrophic balance. The approxi-
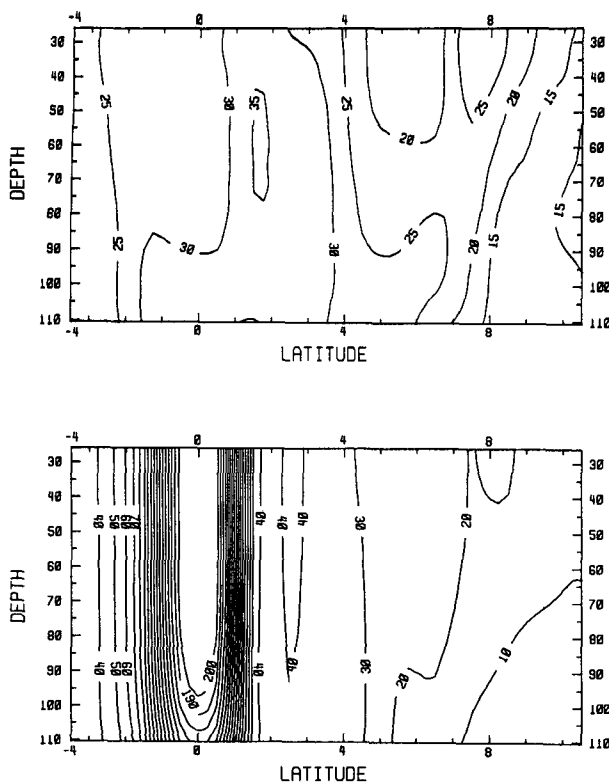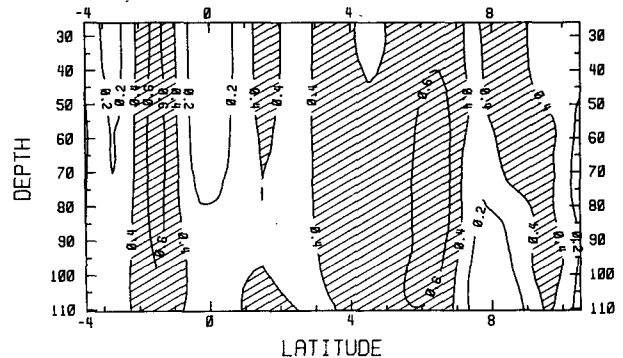
FIG. 7. The correlation between DAL observed and geostrophic zonal velocities. The means removed previous to this calculation are those of Figs. 3a and 5a. Values greater than 0.4 are different from zero at 95% confidence, and are crosshatched.

mate balance holds for vertical shear of velocity as well. This balance is in agreement with Lukas and Firing (1984) who, using PCM velocities and CTD densities from the same experiment, found the mean zonal velocity above 300 m between 4°S and 4°N to be geostrophically balanced. As in their geostrophic profile, Fig. 5a shows the EUC extending closer to the surface than does the observed profile. Also, the southern boundary of the NECC is further north in Fig. 5a than in Fig. 3a. None of the ageostrophic velocities of Fig. 5b are statistically significant due to the very high noise in the geostrophic calculation (i.e., the CTD densities) near the equator. Confidence limits are calculated in general assuming the departures from geostrophy of all profiles are independent and normally distributed. This independence was tested by calculating the time lag covariance of the profiles, and found to hold true at all latitudes except 2.5°–3.5°S and 2.5°–4.5°N, where up to five pairs of profiles closely spaced in time may not be completely independent. The effect of this on the statistics is small, hence the assumption of independence. Ageostrophy near the surface at the equator is significant at 95% confidence when viewed as vertical shear (see section 4b).

In contrast to the mean field, the time dependent field (that which is left after the mean is removed) is not closely geostrophic. Near the equator the geostrophic velocity variance is much greater than the observed velocity variance (Fig. 6). This cannot be due to noise in the geostrophic calculation as this noise is not large enough (see above). The probable source is high-frequency internal waves contributing to the density signal (see section 5b). The variance mismatch between geostrophic and observed velocities makes a geostrophic balance unlikely. However at two or more degrees from the equator the variances are more closely matched and the correlation between geostrophic and observed velocities is a reasonable test of geostrophy. Figure 7 shows the time correlation between the time dependent fields of zonal and geostrophic velocities.

FIG. 6. The standard deviation of (top) observed and (bottom) geostrophic zonal velocity in cm s^{-1}.

The observed velocity variances are in general far greater than the DAL noise levels estimated from the comparison to the PCM data and so must be considered real. Removing the mean from velocities at each longitude rather than from all velocities together does not change the results of Fig. 7 materially. Correlations of 0.4 and greater are significantly different from zero at 95% confidence, assuming all profiles are independent as before. It is apparent that geostrophy does not dominate the observations near the equator. North of 3°N higher correlations exist, but even there the flow cannot be characterized as predominantly geostrophic. For example, the fraction of the observed velocity variance which can be predicted from the measured geostrophic values using a linear least-mean-square error model is equal to the correlation squared. By this criterion even the highest observed correlations of 0.75 would allow only half of the observed velocity variance to be predicted using geostrophic calculations. At 3.5°S, values of 0.4 are found. It is possible that the alternating high and low values from 3.5°N to 3.5°S are due to time-dependent meridional advection of the geostrophically balanced mean flow (Fig. 3a); the low correlations at ±2.5° correspond to areas of low mean U_y. North of the NECC from 11°N to 20°N the statistical significance of all averaged quantities is low since only about seven observations are available in each 1° latitude bin. However, when averaged over all latitude bins north of 11°N, the rms observed velocity was 2.4 ± 0.5 times the rms geostrophic velocity; for shears the factor was 5.0 ± 0.9. This qualitatively recalls the similar finding of Regier (1982a) who, in the Sargasso Sea near 31°N, found observed shears to be twice the geostrophic shears.

4. Ageostrophy

Both the mean and the time dependent DAL zonal velocity fields show at least some statistically significant ageostrophy. This ageostrophy must be balanced by one or more additional momentum terms, some of which can be examined with the present data. The division of the data into mean and time dependent fields is actually a division into two time scale bands: scales longer than one year (the mean) and scales shorter than a year. The additional momentum terms which are important need not be the same for both: here meridional acceleration is compared to time dependent ageostrophy and the meridional advection of meridional momentum to mean ageostrophy. These pairings are arrived at through a combination of scaling arguments and limitations imposd by the nature of the dataset. The horizontally frictionless meridional momentum equation is

$$v_t + uv_x + vv_y + wv_z + fu = \frac{-1}{\rho_0} P_y + \frac{1}{\rho_0} \tau_z{}^y,$$

where subscripts denote partial derivatives. Friction terms and w are unmeasured, as is v_x, since v decorrelated between successive observations at different longitudes. Neglecting these for the moment, we then have

$$v_t + vv_y + fu = \frac{-1}{\rho_0} P_y + \frac{1}{\rho_0} \tau_z{}^y.$$

We now determine whether the observed ageostrophy can be balanced by the remaining momentum terms.

a. Time dependent ageostrophy

Figure 8 shows that vv_y is negligible in the time dependent field. τ^y can be estimated from the wind measurements at the equatorial moorings. Its standard deviation (using $\rho = 1.2$ kg m^{-3} and $C_D = 1.25$) is 0.15 dyn cm^2. If this stress is applied as a body force to a mixed layer 50 m deep ($\tau_z{}^y = \tau^y/H$) the resulting momentum root variance is 21×10^{-6} cm s^{-2}, again small relative to the terms in Fig. 8. Thus we examine the balance of ageostrophy with meridional acceleration. Unfortunately the meridional velocities were found to be uncorrelated between repeat samplings so no directly measured time derivative is available from the DAL data, and the assumed balance cannot be tested at any given instant. However the statistics of meridional acceleration are available from moored current-meter measurements. The question addressed is then whether the variance of the meridional acceleration is large enough to balance the variance of the ageostrophic momentum term. Starting with the simplified momentum term. The momentum equation, as simplified above, is

$$v_t + fu = \frac{-1}{\rho_0} P_y,$$

in which all flow variables have had their time means removed. Integrating in y between CTD stations as before gives

$$V_t = -\bar{f}(U - G),$$

where $\bar{f}$ is the averaged f, G the geostrophic zonal velocity [i.e., the far right term in (3.2)], and capitalized
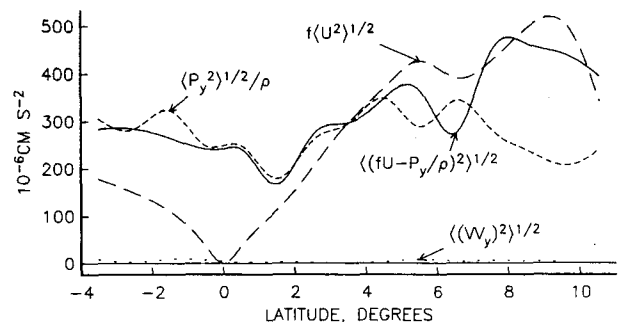

FIG. 8. The standard deviation of various terms in the meridional momentum equation, in cm s^{-2}.

velocities denote a meridional average between CTD stations. This equation obtains at each instant. Denoting a time average over the available data by angle brackets:

$$\langle V_t^2 \rangle = \bar{f}^2 \langle (U - G)^2 \rangle. \qquad (4.1)$$

The ageostrophic variance term on the right is available from the DAL and CTD data. The $\langle V_t^2 \rangle$ is not available from the DAL because the process was not correlated between successive samples at the same location, but $\langle V^2 \rangle$ is. Here $\langle V_t^2 \rangle$ is available from the MCM data, but that value cannot be substituted directly into (4.1) since the MCM data includes small spatial-scale variance which is averaged out of the DAL data. The ratio of acceleration variance over velocity variance defines a frequency scale,

$$\frac{\langle V_t^2 \rangle}{\langle V^2 \rangle} = \omega_0^2. \qquad (4.2)$$

If V has a stationary spectral shape [i.e., $S_{VV}(\omega_1)/S_{VV}(\omega_2)$ is constant over time], then ω_0 will be a constant. The frequency scale ω_0 may also be obtained from the DAL and CTD data using (4.1):

$$\frac{\bar{f}^2 \langle (U - G)^2 \rangle}{\langle V^2 \rangle} = \omega_0^2. \qquad (4.3)$$

Equations (4.2) and (4.3) afford two ways of calculating the frequency scale ω_0. Using (4.2) we can calculate ω_0 from moored current meter (MCM) data. With (4.3) we can calculate ω_0 indirectly through the assumed momentum balance (4.1), using the DAL and CTD data. If acceleration exactly balances ageostrophy, then the two estimates of ω_0 from the data must be equal. Of course the converse, that if the two estimates of ω_0 are equal the balance is exact, is not necessarily true. However, if the directly measured ω_0 of (4.2) is less than the ω_0 of (4.3) required by the assumed momentum balance, then that balance cannot exist, because the frequency scales of meridional motion and the resulting accelerations are too small to balance the ageostrophy.

Figure 9 shows the two frequency scales as a function of latitude. The curve is drawn over the ω_0 of (4.3) calculated from the variance of the DAL velocities at 52 and 104 m. Isolated points represent the ω_0 of (4.2) calculated from MCM velocities at 50 and 100 m. The error bars are 95% confidence limits calculated using the assumption of independent profiles (but not depths) as before for the DAL ω_0, and for the MCM ω_0 using ω_0^{-1} itself as an estimate of the decorrelation time of the velocities in (4.2). The three moorings near the equator are the NORPAX moorings, and the three in the NECC were deployed by D. Halpern from November 1977 to March 1978. These last are not concurrent with the DAL data, but year to year changes in variance should not affect the calculation if V has a stationary spectral shape. Note that the MCM ω_0 of (4.2) used
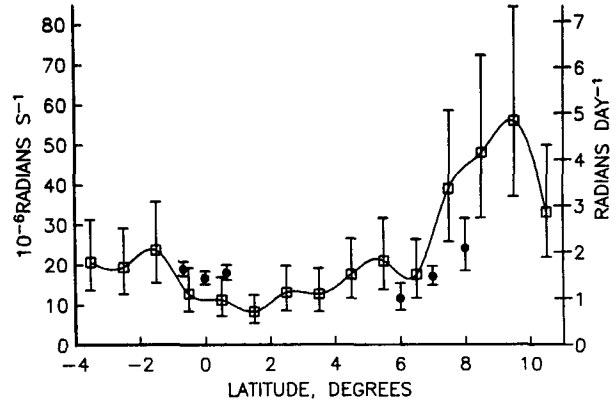

FIG. 9. The frequency scales ω_0 derived in Eqs. (4.2) and (4.3). The required ω_0 derived from the DAL data via (4.3) is the solid curve, while the measured ω_0 of (4.2) from the current meters is plotted as isolated points. The error bars are 95% confidence limits.

measurements of velocity at a point, whereas (4.3) requires velocities averaged over 1° of latitude. This spatial averaging may bias ω_0. When the same averaging is performed in the wavenumber–frequency domain on a Garrett and Munk internal wave spectrum with j_* set to three (Munk 1981) the change in ω_0 is about -30% at 8°N.

The values of ω_0 from the moorings at the equator are higher than the ω_0 values required for a balance of acceleration with ageostrophy. Therefore there is more than enough acceleration present to effect such a balance at the equator. The required frequency scale increases with latitude away from the equator, reflecting increasing ageostrophic momentum variance (Fig. 8) while $\langle V^2 \rangle$ remains roughly constant. In the NECC the measured ω_0 became slightly smaller than the required ω_0, which would imply that acceleration cannot balance ageostrophy there. However for absolute velocities the ageostrophic variance in (4.3) includes both navigational noise in the Doppler velocities and the velocity variance of the geostrophic level of no motion, taken here to be from 300 to 500 m. These extra variances would of course have no balancing acceleration forces in the surface layers, and would bias the required ω_0 upwards. The navigational noise calculated in the Appendix closely accounts for the observed discrepancy; for variances averaged between 5.5° and 8.5°N the adjusted ω_0 is about 20×10^{-6} rad s^{-1}. Therefore if the other terms of the momentum equation can truly be neglected, then the meridional acceleration in the NECC must closely balance the time-dependent ageostrophic velocities. The above results are unchanged if shears are used instead of absolute velocities.

b. Mean ageostrophy

In previous sections the analysis is cast in terms of absolute velocities. The ageostrophy of the mean velocity field, however, is not statistically significant at

the equator due to the large geostrophic velocity variances there (Fig. 6b). The variance of geostrophic shear is relatively small at the surface near the equator, so that the vertical shear of the ageostrophy is statistically significant there. In effect the fluctuating geostrophic velocities have larger vertical scales than the means and so are suppressed by the vertical derivative, leading to smaller standard errors of the mean for geostrophic shears. Hence the mean ageostrophy at the equator will be analyzed in terms of vertical shear. The ageostrophic shear considered occurs in the surface "mixed" layer, which is generally 60 m deep. In the mixed layer density is uniform in the vertical, yielding vertically constant geostrophic shear according to the thermal wind relation. The same mixing tends to suppress velocity shear, leading to a large difference in observed and geostrophic vertical shears.

The ageostrophic shear is compared to the non-linear momentum term $\overline{(VV_y)}_z$, neglecting for the moment the wind stress term, τ^y_{zz}/ρ_0, and also the acceleration, $\overline{V_{tz}}$, as well as the previously neglected terms. (Here an overbar denotes an average over the year of data of a flow variable.) Note that the nonlinear term includes the mean product of the fluctuating velocities. If the mean were a true block average over a year of well-sampled data the neglect of acceleration would be easily justifiable. However, V decorrelated between repeat samplings, so what is obtained in the mean here is not a block average over time but an ensemble average of independent measurements. On this basis and with the limited number of independent measurements available, the standard error of $\overline{V_{tz}}$ is expected to be of about the same magnitude as the observed ageostrophy. Therefore, a comparison between $\overline{(VV_y)}_z$ and $\overline{f(U_z - G_z)}$ will in this case be contaminated by a large noise term, $\overline{V_{tz}}$, which in a true yearly mean would be negligible. There are in addition the friction and zonal gradient terms neglected earlier, which may be significant in a true yearly mean.

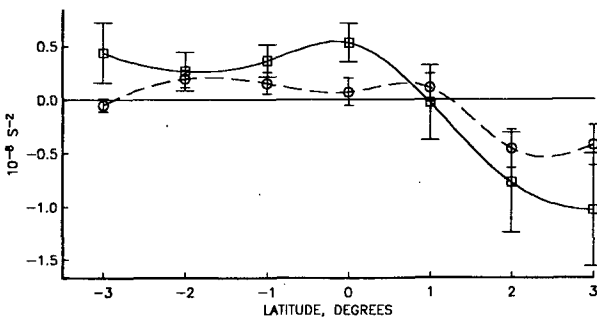The comparison of the vertically differentiated momentum terms above is presented in Fig. 10.

FIG. 10. The mean, as in Fig. 3, of meridional momentum terms vertically differentiated between 26 and 52 m depth. The dashed line is $-\overline{(VV_y)}_z$ while the solid line is $\overline{f(U - UG)}_z$ smoothed over 2° latitude.

$\overline{f(U_z - G_z)}$ is plotted with $-\overline{(VV_y)}_z$; if the terms balance in the ocean the plots should overlie one another. Also plotted are the 95% confidence limits at each data point, calculated with the previous roughly verified assumption of independent profiles. The formal error bars are large and overlap at all points but two. Nevertheless, the advection term is seen to have systematically smaller amplitude than the measured ageostrophic term, suggesting that over this band of latitudes (3°S to 3°N) some other term(s) in addition to $\overline{(VV_y)}_z$ must be important in balancing the ageostrophic shear.

It is possible that τ^y is important in balancing the mean ageostrophy. From the mooring wind measurements the mean surface stress, τ_o^y, is 0.03 dyn cm^{-2}. If this stress is distributed as a body force over a mixed layer of depth H then $\tau_z^y = \tau_o^y/H$ for $z > -H$. As the momentum terms in Fig. 10 have been vertically differentiated, this distribution of τ^y would make no contribution to the balance shown, since τ^y_{zz} is zero except at $z = -H$. If for the sake of argument we choose τ^y_{zz} to be constant for $z > -H$ with $\tau_z^y = \tau^y = 0$ at $z = -H$, then $\tau^y_{zz} = 2\tau_o^y/H^2$. For $H = 50$ m, $\tau^y_{zz}/\rho_0 = 0.23 \times 10^{-8}$ cm s^{-2}, which is large enough to be important in the balance of Fig. 10. While τ^y_{zz}/ρ_0 cannot therefore be ruled out as a significant term, it is unlikely that it makes up the difference between $\overline{f(U_z - G_z)}$ and $\overline{(VV_y)}_z$. This difference changes sign at the equator, whereas climatologically τ_o^y is fairly constant within 3° of the equator at this longitude (Legler and O'Brien 1984).

5. Discussion

a. Equatorial geostrophic balance

The meridionally differentiated geostrophic balance,

$$u_{eq} = \frac{-1}{\rho_0 \beta} P_{yy}, \qquad (5.1)$$

where $\beta = f_y$, is used at the equator between 1°S and 1°N in all the calculations of the previous sections. This is equivalent to averaging traditional geostrophic velocities,

$$u = \frac{-1}{\rho_0 f} P_y, \qquad (5.2)$$

across the equator when discrete density data is used (Tsuchiya 1983). Consider three CTD stations at 1°S, 0° and 1°N, which give pressures P_{-1}, P_0 and P_1, respectively, at some depth as a function of time. Application of (5.1) requires that the continuous y derivatives be turned into finite differences,

$$u_{eq} = \frac{-1}{\rho_0 \beta d^2} (P_{-1} - 2P_0 + P_1),$$

where the distance d is one degree of latitude here.

Rearranging terms,

$$u_{eq} = \frac{-1}{2\rho_0} \frac{2}{\beta d} \left[\frac{P_1 - P_0}{d} - \frac{P_0 - P_{-1}}{d} \right]$$

or

$$u_{eq} = \frac{-1}{2\rho_0} \left[\frac{P_1 - P_0}{f_{0.5}d} + \frac{P_0 - P_{-1}}{f_{-0.5}d} \right]$$

where $f_{0.5} = \beta d/2$ is f at $0.5°N$. This of course is the average of traditional geostrophic velocities,

$$u_{eq} = \frac{1}{2} [u_{0.5} + u_{-0.5}].$$

If $u_{0.5}$ and $u_{-0.5}$ are considered to be made up of S, a velocity which is symmetric about the equator, and A, an antisymmetric velocity, then the equatorial geostrophic calculation filters out A and retains S. Note that if A is negligible, using (5.1) will be equivalent to using (5.2). The resulting plots, however, will be equivalent only if the equatorial value u_{eq} is plotted at both $0.5°N$ and $0.5°S$, as are $u_{0.5}$ and $u_{-0.5}$. This is the practice used in this paper. If u_{eq} were plotted at the equator a narrower, slower EUC core would result compared to the plot of the traditional calculation, even when the two calculations were equivalent.

b. Noise near the equator

In the present data, use of (5.1) instead of (5.2) reduced the mean departures from geostrophy at the equator (Fig. 5b, root-mean-squared over depth) from 29 to 18 cm s^{-1}. Similarly, it reduced the time dependent ageostrophic root variance from 217 to 192 cm s^{-1}. As the retained variance is S and the filtered variance is A, this implies that the variance of S is three to four times that of A (192^2 vs 217^2–192^2). It is likely that this dominance by S is due at least in part to internal wave noise contaminating the density data. Noise in the density observations evenly distributed over the three CDT stations ($1°S$, $0°$, $1°N$) and uncorrelated between stations (i.e., white, or at least spatially aliased noise) would contribute three times as much variance to S as to A. In effect ageostrophic velocities on either side of the equator are positively correlated through their common use of the density measurement on the equator. Decomposing the independently measured geostrophic velocities at $1.5°S$ and $1.5°N$ yields a more even balance between S and A; at these latitudes the variance of S is only 20% greater than that of A. Also Fig. 8 shows that the variance of the momentum term P_y/ρ, which when divided by $-f$ gives the geostrophic velocity (5.2), is roughly constant with latitude and greater than the variance of fU within $2°$ of the equator. Therefore the observed ageostrophy near the equator has statistics consistent with those expected of uncorrelated noise in the density data.

The ageostrophic root variance observed amounted to 70 cm s^{-1} at $1.5°S$, 190 cm s^{-1} about the equator

using (5.1), and 45 cm s^{-1} at $1.5°N$. These are greater than might be expected from large-scale oceanographic processes. For example, Knox and Halpern (1982) show intermittent oscillations in their meridional velocity time series with about a 15-day period and a maximum 50 cm s^{-1} amplitude. Since the variance of a sinusoid is half the amplitude squared, and the features are intermittent, the rms velocity over the year of data is perhaps 20 cm s^{-1}. Such a wave would contribute [via (4.1)] an ageostrophic signal of 76 cm s^{-1} at $0.5°$ and 25 cm s^{-1} at $1.5°$, signals too small to be seen in the observed variance. Given this and the fact that the variance exhibits symmetries expected of random noise (previous paragraph), it is likely that this variance is mostly spatially-aliased internal wave noise rather than larger-scale well-sampled features. (Note that the spatial aliasing is not producing spurious ageostrophy, but rather the ageostrophy is characterized by spatial scales smaller than $1°$ of latitude.) Hayes (1982) and Moum et al. (1987) emphasize the importance of averaging out such noise before applying geostrophy to individual density sections across the equator. Section 4a further shows that these waves are of high frequency, much higher than the local f, so that their meridional pressure gradients must be balanced by meridional acceleration. It is theoretically possible that were these spatially aliased high frequency waves filtered from the density data, the underlying large-scale fluctuations would be found to be geostrophically balanced. It is possible that filtering in time will be needed as well.

North of $4°N$, Fig. 8 shows more variance of fU than of P_y/ρ. This precludes the possibility of internal wave density noise obscuring underlying geostrophic fluctuations. The only possible conclusion is that the large-scale velocity fluctuations are predominantly not geostrophic. Since the frequency scale ω_0 found in the NECC (Fig. 9) approximates the local f ($= 18 \times 10^{-6}$ s^{-1}) it is likely that inertial oscillations contribute to the observed velocities, and hence the ageostrophic velocities.

c. Monitoring the equatorial currents

Part of the intent of the NORPAX shuttle was to explore our ability to monitor the zonal currents near the equator using density data and an assumed geostrophic balance. Since the purpose of 'monitoring' is generally to resolve the fluctuations in the flow, it is crucial to keep in mind the differences between the mean and the fluctuating flows before drawing conclusions about our ability to monitor the currents.

The standard deviations of the observed flow (Fig. 6a) are in general smaller than the mean flow features (Fig. 3a); in particular the mean velocity of the Equatorial Undercurrent is twice as big as its standard deviation. The fluctuating flow has been found to be at best only partly geostrophic, generally less so closer to
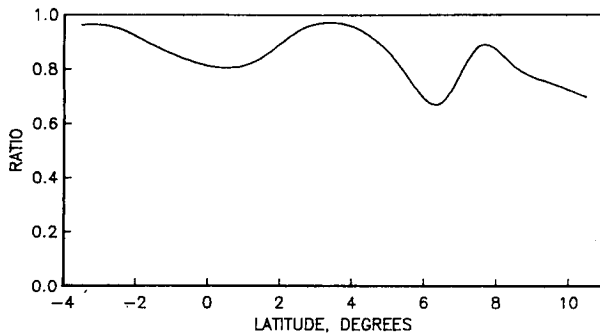
FIG. 11. The ratio of the variance of the vertical mean (26–117 m) of zonal velocity over the vertical mean of the variance of zonal velocity.

the equator where f goes to zero and the rms geostrophic velocity gets large (Fig. 6b). Finally, Fig. 11 shows the variance of the vertical mean of u from 26 to 117 m depth over the average of the total variance of u in the same depth range. Very little variance is lost in taking the vertical mean, showing that the fluctuating flow is dominated by vertically uniform flows, even though the mean flow (Fig. 3a) is highly sheared.

A number of conclusions can be drawn from these statistics. First, while the fluctuating flows observed in the NORPAX Shuttle were only slightly geostrophic near the equator, more heavily sampled sections smoothed to reduce the small-scale internal wave noise mentioned in section 5b could possibly resolve larger-scale geostrophically-balanced fluctuations. Second, such a smoothed section across the equator at any given time can be geostrophically balanced simply because the flow is likely to be dominated by its geostrophic mean. Such a finding of instantaneous geostrophy does not imply that the flows can be monitored geostrophically; that would require the fluctuating flow to be predominantly geostrophic, a more stringent condition. Lastly, the statistics of the vertical shears near the surface contain relatively little information about the fluctuating absolute velocities, since these are dominated by fluctuations having little vertical shear in the top 120 m. Therefore an experiment cannot determine how well we can monitor tropical flows geostrophically unless it measures absolute velocities as well as densities with sufficient repetition in time to distinguish the fluctuating from the mean flow.

6. Summary

The Doppler acoustic log data from the NORPAX Hawaii to Tahiti shuttle has been presented and analyzed as meridional sections across the equator. The time-averaged section shows the classical zonal currents and to a large degree confirms the expected meridional circulation. Comparison in the Appendix with the concurrent profiling current meter data has produced error estimates for both datasets. The DAL data used to confirm that the zonal velocity and meridional pres-

sure gradient within 4° of the equator are in close geostrophic balance, as found by Lukas and Firing (1984), and to show that the balance extends to 10°N. Ninety-five percentile significant departures from geostrophy are found in terms of vertical shear in the mixed layer above the EUC. This departure occurs where density has been relatively well mixed in the vertical, resulting in vertically-uniform geostrophic shear, while zonal velocity shear is suppressed by the same mixing. This mean geostrophic imbalance appears to be only partially compensated by the meridional advection of meridional momentum, but the presence of poorly averaged accelerations in the mean precludes a definite conclusion as to whether other momentum terms are necessary to complete the mean balance.

The time-dependent flow, remaining after the above mean is removed, is in general not geostrophic near the equator, and is only partly geostrophic north of 3°N through the NECC. Nowhere would it be possible to geostrophically predict more than half the observed velocity variance using the present data. North of the NECC to 20°N the observed velocity variance is 2.5 times that of geostrophic velocity, in keeping with Regier's (1982a) results in the Sargasso Sea with a similar instrument. Moored current meter data was used to estimate the frequency scale of meridional acceleration variance in the EUC and the NECC. The frequency scales obtained from DAL velocities indicate that there is more than enough acceleration variance to balance the ageostrophy in the EUC, and barely enough in the NECC. If other momentum terms are negligible, the NECC must have a very close balance between pressure, Coriolis force, and acceleration.

The very large variance of geostrophic velocity near the equator is likely due to high-frequency spatially aliased internal waves contaminating the density data and hence the pressure calculations. These non-geostrophic pressure gradients, when divided by the small f near the equator, produce large, spurious, geostrophic velocities which contribute to the lack of geostrophic balance in the time-dependent flow there. This explanation for a lack of geostrophic balance cannot be applied north of 4°N, where there is an excess of observed velocity variance relative to geostrophic velocity variance. Since the observed frequency scale in this area approximates the local f, this excess velocity variance is probably due to near inertial internal waves.

Finally, an experiment to determine whether the equatorial currents can be monitored geostrophically must both sample the time variability of the currents and filter out internal wave contamination of the density data.

APPENDIX

A Comparison of DAL with PCM and MCM Data

A comparison of the Doppler acoustic log (DAL) data with that of Firing's profiling current meter (PCM) and Halpern and Knox's moored current meters (MCM) is presented in order to establish the degree of reliability of the DAL data. There are two goals; first an estimate of the noise levels for this set of DAL data is produced, and second the comparison with the PCM gives an expected mutual noise level to be found in any comparison between those two data sets. In particular, it is desired to know if the continuous profiling of the DAL could provide more accurate profiles with which to examine geostrophic balance and other ocean dynamics near the equator than can the point measurements of the PCM or the MCM.

The MCM data used consisted of single 30-minute averages of velocity at 50 and 100 m depths from either of the two off-equator mooring sites (153°W, 0°40′S and N). Eleven of these two point vertical profiles were extracted for periods in time during which the ship (steaming north or south and operating the DAL) passed the latitude of the mooring while within 0.5 degrees longitude. The single five-minute block-averaged DAL absolute velocity profile taken at that time was interpolated to 50 and 100 m depths and compared to the MCM profile. As the ship steamed at 10 to 12 knots, the five-minute average corresponds to a spatial average over somewhat less than 2 km, or 0.02° for relative velocity. The absolute velocity is necessarily spatially averaged between adjacent satellite fixes, which may be from 20 minutes to 3 hours apart. The analysis was repeated using DAL data averaged over 0.4° latitude and MCM data averaged over the equivalent time span, about two hours.

The PCM data consisted of 280 profiles taken on stations at integral latitudes from 4°S to 10°N and various longitudes, with no fewer than 13 profiles from any one latitude. All profiles used were assigned Firing's highest (subjective) quality rating (Firing et al. 1981). These were interpolated in depth and compared to DAL data taken as the ship approached and left the PCM station, averaged over the 1° of latitude centered at the PCM profile.

The analysis of all three comparisons proceeded similarly. No statistical distinction was made between longitudes, as no differences between them were readily apparent (see Section 3). Therefore the data were located in time, latitude, and depth only. First time-mean profiles as a function of latitude and depth were extracted from each data type (hereafter called the mean fields);

$$\bar{A}(\phi, z) = \frac{1}{N} \sum_{i=1}^{N} A(\phi, z, t_i);$$

$$A'(\phi, z, t) = A(\phi, z, t) - \bar{A}(\phi, z).$$

Here $A(\phi, z, t)$ is the acoustic data, and P will be either PCM or MCM data. Then each pair of profiles (DAL and corresponding other data) was differenced;

$$D(\phi, z, t) = A'(\phi, z, t) - P'(\phi, z, t).$$

These difference velocities were not used directly, but were averaged in the vertical to form a mean difference velocity and vertically differentiated to form a difference vertical shear;

$$\bar{D}(\phi, t) = \frac{1}{M} \sum_{i=0}^{M} D(\phi, z_i, t); \qquad (A1)$$

$$D_z(\phi, \zeta_n, t) = \frac{1}{z_{n+1} - z_n} [D(\phi, z_n, t) - D(\phi, z_{n+1}, t)];$$

$$\zeta_n = \frac{1}{2} (z_n + z_{n+1}). \qquad (A2)$$

The root-mean (over all profiles) square values of these two quantities were then calculated (hereafter called the rms mean difference and rms shear difference). These quantities are affected in quite different ways by errors in the DAL data. The mean difference is a difference of velocities relative to the earth, or absolute velocities, and contains errors in determining the ship's velocity by means of satellite navigation, while the shear difference does not. The PCM data was referenced by Firing et al. (1981) to the fixed earth by adding a vertically constant velocity to each station so that the velocity, averaged between 300 and 500 m depth, was zero.

The mean fields extracted above from the various data types agreed well. The differences between the MCM and the DAL mean fields were on the order of 1-4 cm s^{-1} for meridional velocity, v, and 1-8 cm s^{-1} for zonal velocity, u. These differences are not different from zero at 95% significance, assuming the differences are uncorrelated in time. The PCM mean field as a function of depth and latitude also was not significantly different from that of the DAL, with differences of the same magnitude (Fig. 12). An exception was found in the mean difference velocities at 9° and 10°N, where the DAL mean shows some 6 cm s^{-1} excess northward velocity; but this difference, while significant by itself, it is not significant when considered as one of many observed differences. Note that as expected the differ-
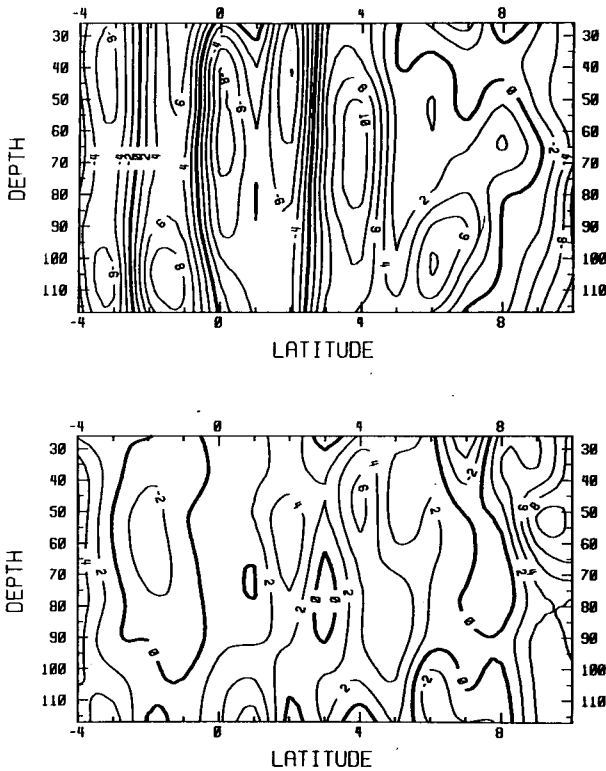
LATITUDE

LATITUDE

FIG. 12. The difference of the DAL less the PCM velocities in cm s^{-1} averaged over all profiles, with zonal velocity (top) positive eastward and meridional velocity (bottom) positive northwards. Each latitude is averaged from 13 to 23 profiles.

ences between the DAL and PCM data means are well correlated in the vertical, indicating that a significant amount of the difference is due to errors in the navigational methods of one or both datasets. Assuming no systematic errors in the satellite navigation of the DAL data, the vertical means of these differences can be taken as a measure of the mean drift at the PCM 300–500 m reference level. Such a mean is shown in Fig. 13. The zonal flow implied is westward between the equator and 2°N, with eastward flow at 1° and
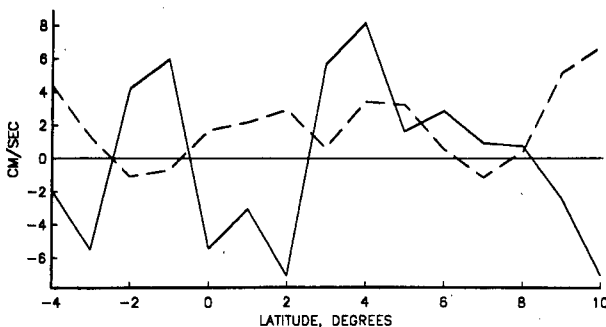

FIG. 13. The vertical mean of the differences of Fig. 12. Zonal velocity is the solid line, meridional the dashed.

TABLE 1. The rms difference for vertical mean and vertical shear velocity, in (meridional, zonal) pairs. N is the number of independent samples in each comparison.

Comparison	Vertical mean (cm s^{-1})	Vertical shear (cm s^{-1}/m)	N
PCM-DAL 1° ave	(12, 18)	(0.22, 0.24)	280
MCM-DAL 0.4° ave	(8, 16)	(0.16, 0.22)	11
MCM-DAL 0.02° ave	(11, 20)	(0.14, 0.18)	11

2°S, and at 3° and 4°N. Again the differences are not significantly distinguished from zero at 95% confidence by this data, the confidence intervals being (5.2, 8.0) cm s^{-1} for (v, u).

The rms differences for the vertical means and shears [(A1) and (A2)] of all three comparisons are presented in Table 1. The statistics have been averaged over latitude and depth for compactness and statistical stability. Considering first the two MCM comparisons, note that the only difference between them is the extent to which the DAL and the MCM data were averaged; in one case over 0.4° and in the other 0.02° of latitude, the MCM data being averaged over the same time period used in gathering the DAL data. As averaging of the DAL data increases, the rms mean difference is reduced, but the rms shear difference increases. The decrease in rms mean difference is expected, as erroneous velocities due to inexact navigation tend to cancel over time (although systematic errors are possible as well, see Regier 1982b). However, the increase in rms shear difference cannot be due to an instrument noise; it is assumed that instrument errors decrease or remain constant with averaging. This will be true if the DAL shear noise characteristics are spatially homogeneous in the average, which is reasonable over 0.4° latitude. Therefore the increased difference must be due to some real difference in the ocean as measured by each instrument. The only change in such differences between the two comparisons was the extent to which the data were spatially averaged, therefore the increased shear difference is due to the increased meridional displacement of the DAL data in the average; in effect the difference between a point measurement and a meridional average.

The rms differences for the PCM–DAL comparison are shown in Figs. 14 and 15, and included in Table 1. The rms mean difference in Fig. 14 is constant with latitude except for zonal velocity difference at the equator. This increased rms difference cannot be conveniently attributed to particular stations and is apparently real. Zonal rms shear difference (Fig. 15) is also observed to be greater near the equator, particularly in the EUC, as well as in the high vertical shear region of the NECC. The meridional shear differences are more uniform in depth and latitude. Both instruments had increased noise in the areas where the oceanic signal was strong.
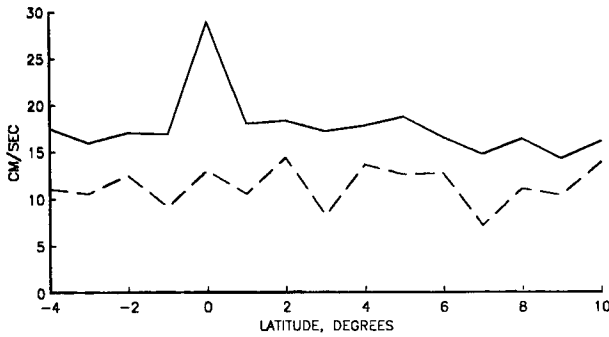
FIG. 14. The root-mean-square difference between DAL and PCM vertically averaged velocities as in Eq. (A1). Zonal velocity is the solid line, meridional is the dashed.

The averaged PCM–DAL rms differences of Table 1 are greater than those of the MCM–DAL 0.4° differences for both mean velocities and shear. This is ascribed both to noise in the PCM measurements and to the greater (1°) meridional averaging of the DAL data in the PCM comparison. Sufficient data were gathered to enable the rms difference variances to be divided into noise levels for each instrument in the following manner. First the time mean (as a function of latitude and depth) of the DAL and of the PCM data is removed as before. Consider the resulting data as measurements of the real ocean with added noise (from whatever source):

$$A_i = Z_i + a_i; \quad P_i = Z_i + p_i$$

where A_i and P_i are the DAL and PCM measurements, Z_i is the real ocean commonly observed by both instruments, and a_i and p_i are the noises. Assume that a_i and p_i are uncorrelated, since the measurements were taken independently. Assume further that the noises have zero mean and are uncorrelated with the real ocean. Then the difference variance is (with angle brackets implying an average over an infinite amount of data)

$$\langle (A_i - P_i)^2 \rangle = \langle a_i^2 \rangle + \langle p_i^2 \rangle$$

while the difference of variances is

$$\langle A_i^2 \rangle - \langle P_i^2 \rangle = \langle a_i^2 \rangle - \langle p_i^2 \rangle.$$

From these the noise variances are obtainable; for example (dropping the subscripted i)

$$\langle p^2 \rangle = \frac{1}{2} [\langle (A - P)^2 \rangle - \langle A^2 \rangle + \langle P^2 \rangle].$$

For finite amounts of data, the above becomes an estimate. The mean square error of the estimate can be found to be

$$\langle (\langle p^2 \rangle - \langle \hat{p}^2 \rangle)^2 \rangle$$

$$= \frac{1}{N} [\langle Z^2 \rangle (\langle p^2 \rangle + \langle a^2 \rangle) + \langle a^2 \rangle \langle p^2 \rangle]$$

where $\langle \hat{p}^2 \rangle$ is the estimate of $\langle p^2 \rangle$, and N is the number of independent samples.

Any variance not contained in Z_i, the mutually observed ocean, is considered noise by this analysis. The PCM point measurements will contain variance due to small-scale features which are averaged out of the 1° DAL average. This measured variance will be attributed to noise in the PCM, as it is not observed by the DAL. The resulting PCM noise level will therefore be the noise expected when the PCM point measurement is used as a measure of flow averaged over a 1° section, the averaging interval appropriate for geostrophic calculations using the NORPAX data.

Note that nonzero correlation between the noise and the real ocean will shift estimated noise variance from one instrument to the other. One source of such correlation is the correlation of nonzero velocities in the PCM reference layer (which become errors in PCM absolute velocities) with shallower velocities. Vertical correlation of 50 and 250 m MCM velocities indicates that this could be a significant problem for zonal velocities, at least near the equator. The vertical correlation was positive, which would in this analysis shift noise variance from the PCM to the DAL.

The calculated DAL and PCM noise levels for mean velocity and shears over 13 and 52 m depth are presented in Table 2, with rough 95% confidence ranges for the rms noise estimates and with the standard deviations of the original data. The DAL rms errors for mean velocities are comparable to those of the PCM,

FIG. 15. The root-mean-square difference between DAL and PCM vertical shears as in Eq. (A2). The units are cm s⁻¹/m. (Above) zonal shears; (below) meridional.
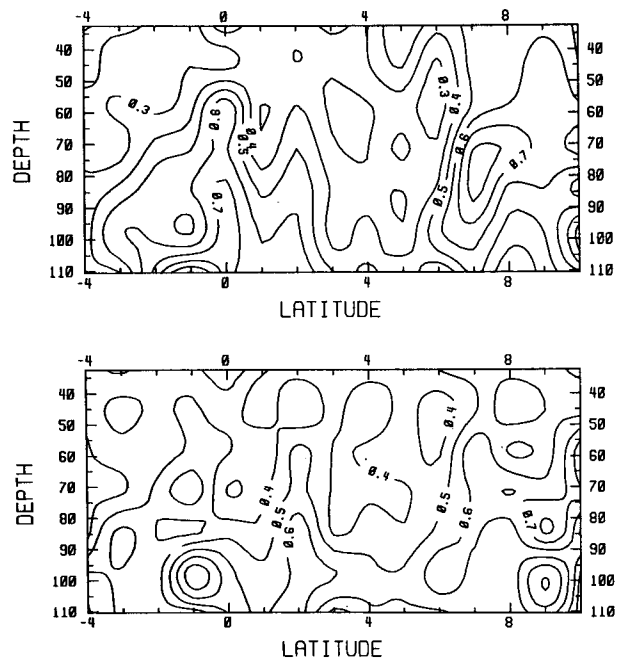
TABLE 2. Error estimates for the PCM and DAL instruments, with 95% ranges and the total standard deviation of the observations for each. Shears have been calculated for two different vertical separations. There are 280 independent samples for vertical mean velocity, and an estimated 560 for vertical shear.

	DAL–PCM Std. dev.	PCM Std. dev.	PCM noise		DAL Std. dev.	DAL noise	
			Rms	95% range		Rms	95% range
V mean (cm s^{-1})	12	16	9	8–10	16	7	6–9
U mean	18	22	11	9–13	24	14	12–15
V_z, 13 m (cm s^{-1}/m)	0.50	0.57	0.48	0.46–0.49	0.34	0.16	0.10–0.20
U_z, 13 m	0.50	0.60	0.47	0.45–0.48	0.42	0.18	0.11–0.22
V_z, 52 m	0.22	0.31	0.22	0.21–0.23	0.23	0.04	0.00–0.08
U_z, 52 m	0.24	0.38	0.23	0.22–0.24	0.30	0.06	0.00–0.10

at (7, 14) cm s^{-1} for (v, u). The u figure is the larger of the two, subject as it is to compass error on the mostly north and south cruise track.

The shear noise of the DAL is much less than that of the PCM, at (0.16, 0.18) cm s^{-1}/m for 13 m shear and (0.04, 0.06) cm s^{-1}/m for 52 m shear. This last is far less than even the MCM-0.02° DAL rms shear difference. Evidently most of the shear differences between the DAL and the other instruments can be ascribed to those instruments and the meridional averaging of DAL data, or to zonal displacements (in the case of the MCM data). Such low DAL shear noise is not unreasonable. Regier (1982b) calculating expected errors from the DAL instrument characteristics finds the expected rms error for shear over 50 m to be 0.02 cm s^{-1}/m for a single 5-minute (0.02°) average profile. This value is close to the observed precision of the instrument over neighboring profiles; the difference between the data variance and the horizontally lagged covariance extrapolated to zero lag implies that the measurements are reproducible to within (0.03, 0.02) cm s^{-1}/m for (v, u). This noise level is negligible, the more so when averaged over 1° of latitude (about 50 profiles). Calibration errors are expected by Regier (1982b) to be 0.5%, also quite small.

The PCM mean velocity noise of (9, 11) cm s^{-1} compares closely with Freitag and Firing's (1984) estimate of 15 cm s^{-1} rms error for v and u together, derived from comparisons of PCM and MCM measurements. The 52 m shear noise of (0.22, 0.23) cm s^{-1}/m is similar to Freitag and Firing's (1984) PCM-MCM rms difference of (0.25, 0.33) cm s^{-1}/m. Note that these figures are not directly comparable, as here the PCM is tested as a measure of velocity over the 1° meridional scale appropriate for testing geostrophy between the NORPAX shuttle's CTD stations. PCM data is actually available every 0.5° of latitude within 3° of the equator. Use of all these stations would decrease the PCM noise due to the aliasing effect of point measurements.

Both the DAL and the PCM shear noise increased with depth (the vertical mean noise was not calculated over different depth ranges). The DAL rms 13 m shear noise increased by about a factor of two from 26–39

m to 104–117 m depth, while the equivalent PCM noise increased only 20% over the same depths.

The noise variances of the DAL and the PCM data are about half as large as the true oceanic variance for absolute velocities. ('True' oceanic variance may be found from Table 2 by subtracting an instrument's noise variance from the standard deviation of its measurement squared.) This is sufficient to adequately measure the large mean zonal velocities of the region, but the variable velocities are smaller than the mean velocities, and as measured are quite noisy. A comparison between the two data types would have as much noise variance as oceanic variance, so only well-averaged quantities would have much significance. However, the similarity in their error characteristics makes mixing of the two data types (e.g., replacing missing data of one type with data of the other) easily dealt with. For shears the data types have quite disparate noise levels. The PCM has noise variance about twice the oceanic variance while the DAL noise is negligible. The DAL data is therefore more useful for examining vertical shear and its dynamics, notably the thermal wind relation. If the DAL instrument could be combined with a more accurate navigational system, such as the Global Positioning System, far more accurate absolute velocity measurements could be made as well.

REFERENCES

Firing, E., C. Fenander and J. Miller, 1981: Profiling current meter measurements from the NORPAX Hawaii to Tahiti shuttle experiment. Data Rep. 39, H1G-81-2, Hawaii Institute of Geophysics, University of Hawaii, 146 pp.

Freitag, P. H., and E. Firing, 1984: Comparison of profiling and moored current measurements in the equatorial Pacific. J. Geophys. Res., 89, 3724–3728.

Hayes, S. P., 1982: Geostrophic velocity profiles at the equator. J. Mar. Res., 40(Suppl.), 219–229.

Hisard, P., J. Merle and B. Voituriez, 1970: The equatorial undercurrent at 170°E in March and April, 1967. J. Mar. Res., 28, 281–303.

Knauss, J. A., 1960: Measurements of the Cromwell Current. Deep-Sea Res., 6, 265–286.

——, 1966: Further measurements and observations on the Cromwell Current. J. Mar. Res., 24, 205–240.

Knox, R. A., and D. Halpern, 1982: Long range Kelvin wave propagation of transport variations in Pacific Ocean equatorial currents. J. Mar. Res., 40(Suppl.), 329–339.

Legler, D. M., and J. J. O'Brien, 1984: *Atlas of Tropical Pacific Wind-Stress Climatology 1971–1980.* Florida State University, 182 pp.

Lukas, R., and E. Firing, 1984: The geostrophic balance of the Pacific equatorial undercurrent. *Deep-Sea Res.,* **31,** 61–66.

Moum, J., T. Chereskin, M. Park and L. Regier, 1987: A comparison of measured and geostrophic currents at the equator. *Deep-Sea Res.,* **34,** 1149–1161.

Munk, W., 1981: Internal waves and small-scale processes. *Progress in Physical Oceanography,* B. A. Warren and C. Wunsch, Eds., MIT Press, pp. 264–291.

Regier, L., 1982a: Mesoscale current fields observed with a shipboard profiling acoustic current meter. *J. Phys. Oceanogr.,* **12,** 880–886.

——, 1982b: Error estimates for the Doppler acoustic log used in the NORPAX shuttle experiment. (Unpublished.)

Sverdrup, H. U., 1947: Wind-driven currents in a baroclinic ocean; with application to the equatorial currents of the eastern Pacific. *Proc. Natl. Acad. Sci. U.S.A.,* **33,** 318–326.

Tsuchiya, M., 1983: Use of nutrient concentrations for monitoring the equatorial undercurrent. *Trop. Ocean-Atmos. Newslett.,* **20,** 3–5.

Wyrtki, K., and B. Kilonsky, 1984: Mean water and current structure during the Hawaii-to-Tahiti shuttle experiment. *J. Phys. Oceanogr.,* **14,** 242–254.

——, E. Firing, D. Halpern, R. Knox, G. J. McNally, W. C. Patzert, E. D. Stroup, B. A. Taft and R. Williams, 1981: The Hawaii to Tahiti shuttle experiment. *Science,* **211,** 22–28.